Experimental Mechanics (2014) 54:199–210
DOI 10.1007/s11340-013-9793-7

Dynamic Behavior and High Speed Machining of Ti-6246 and Alloy 625 Superalloys: Experimental and Modeling Approaches

M. Hokka · D. Gomon · A. Shrot · T. Leemet · M. Bäker · V.-T. Kuokkala

Received: 1 February 2013 / Accepted: 6 August 2013 / Published online: 14 August 2013

Abstract Titanium alloys and nickel based superalloys are used in various demanding applications because of their excellent high temperature properties, especially high strength and good corrosion and fatigue resistance. However, the high strength and hardness at high temperatures combined with strong strain hardening can lead to difficulties in machining of these alloys. Finite element simulations can be used to optimize the cutting conditions and to reduce the machining costs. However, simulations of machining operations require accurate material models that can only be built on reliable experimental data. Also, the mechanical properties of materials can only be measured in a limited range of strain and strain rate at the laboratory scale, from which the material behavior has to be extrapolated to the actual machining range. In this work, the mechanical behavior of Titanium-6246 and a nickel based superalloy, similar to Inconel 625, has been studied in details. The Johnson-Cook material model parameters were obtained from the experimental data and the model was used to describe the plastic behavior of the studied alloys in simulations of orthogonal cutting of the material. The model for the Ni- based superalloy was improved by introducing an additional strain softening term that allows decreasing of the strain hardening rate at large deformations. The preliminary simulation results have also been verified experimentally by comparing the simulation results with machining experiments, and the results of the simulations are briefly presented and discussed. The material models are able to reproduce the serrated chips with split shear bands, but the cutting stresses obtained from the simulations are somewhat higher than those obtained from the cutting experiments. Also, some differences were observed in the chip shape, and further development of the material model and simulations is needed.

Keywords Superalloy · Titanium alloy · High strain rate · Split Hopkinson Pressure Bar · FEM Simulations · Johnson-Cook model · Machining

M. Hokka (✉) · D. Gomon · T. Leemet · V.-T. Kuokkala
Department of Materials Science,
Tampere University of Technology, Tampere, Finland
e-mail: mikko.hokka@tut.fi

A. Shrot · M. Bäker
Institute for Materials, Germany, Technische Universität
Braunschweig, Braunschweig, Germany

Introduction

Titanium and nickel based alloys are widely used in various demanding applications such as aircraft engine components. These alloys are typically characterized by excellent strength-to-weight ratio and high temperature performance, which are needed in the aircraft engines. Other remarkable properties of these alloys are good corrosion, fatigue, and chemical wear resistance. However, processing and machining of these alloys can be extremely challenging due to their mechanical properties and behavior. The high strength and hardness are typically retained to reasonably high temperatures, and therefore the machining forces tend to be high [1–3]. The mechanical behavior of nickel based superalloys is typically characterized by strong and rapid strain hardening, which can further increase the cutting forces. In addition to the mechanical strength, poor thermal conductivity of these alloys can result in adiabatic heating and increased tool temperatures, which again can significantly increase the costs of the finished components due to rapid tool wear. Furthermore, the formation of long continuous chips instead of short segmented ones can significantly reduce the machinability of the alloy. For certain alloy-tool combinations also the chemical affinity and reactivity of the material, especially titanium, can lead to rapid tool wear due to adhesion between the tool and the workpiece [4]. Finally, the nickel based superalloys commonly contain hard carbides or intermetallic precipitates, which can cause rapid abrasive wear of the tool, again leading to increased machining expenses. For

more detailed description of the machining of nickel and titanium based alloys, see for example refs. [1–3, 5].

Improving the machinability of these alloys can improve the quality of the final products and also reduce the price of the machined components. This can basically be done by developing easier-to-machine alloys, improving tools and their coatings, and by optimizing the machining and cutting conditions in each machining process. The machinability of the alloys can be improved, for example, by suitable alloy development, while recent attempts to improve the machining processes for these alloys have been done, for example, by hybrid machining methods [6] and ultrasonically assisted machining [7, 8]. Optimization of the machining conditions can basically be done by extensive experimental work, but it can also be significantly assisted by finite element simulations. Dong et al. [9] studied the machining of the Inconel 718 alloy and found that the serrated chips are formed at cutting speeds higher than 40 m/min. In their studies they also found that the cutting parameters, such as feed rate and cutting speed, strongly affect the shear stresses, strains, and strain rates that occur during machining. They estimated that for the cutting speed of 40 m/min the shear strains in the chip are around 300 % and the shear strain rates around $2.25*10^5$ s^{-1}. Fang et al. [3] measured the cutting forces for Inconel 718 and Ti-6-4 alloys and found that the cutting forces for both materials decreased as a function of cutting speed and increased with increasing cutting depth. Similar results were reported also by Ulhmann et al. [10]. The results of Dong et al. [9], Fang et al. [3], and Ulhman et al. [10] show that the cutting forces are very sensitive to small changes in the machining parameters such as cutting speed, depth of cut, and feed rate.

There are numerous different testing and measurement techniques and devices described in the literature for experimental machining research. This makes it somewhat difficult to directly compare the results obtained by different researchers. Also the amount of deformation and strain rates that typically occur in machining can be so high that the characterization of the material behavior using simple mechanical testing is extremely difficult. Therefore, a lot of effort has been put on modeling the material behavior and optimizing the machining processes by simulations using finite element methods. However, simulating the material behavior in machining is complicated by the need to extrapolate the known or measured material behavior to much higher deformations and strain rates, as well as the tendency of the material to form adiabatic shear bands during the high speed deformation. Extrapolating the material behavior outside the range where the material model was determined can lead to unexpected results unless the material model has enough predicting power. Therefore, the material models must be chosen properly and the parameters optimized to obtain the best results in the machining conditions. Adiabatic shear bands can be generated in the simulations simply by the local adiabatic heating and the consequent thermal softening of the material, or by using additional damage or strain softening models that can locally soften the material in the heavily deformed primary shear zones. The early work by Ortiz and Quigley [11] and Marusich and Ortiz [12] solved many of the problems related to the strain localization by using adaptive mesh refinement. Using the adaptive mesh refinement, a relatively simple material model, and a fracture criterion based on the fracture toughness $K_{IC,}$ they were able to model and simulate the adiabatic shear banding in high speed cutting of steels. Sima and Özel [13] and Calamaz et al. [14, 15] developed material models based on the Johnson-Cook equation capable of accounting for the reducing strain hardening rate with increasing strain, and were able to simulate the adiabatic shear banding and serrated chip formation in Ti-6Al-4V. Similar results were achieved by Ulhmann et al. [10] using the Johnson-Cook material model and a damage model to simulate similar behavior. For a good review of modeling and simulations of machining, the reader is referred to, for example, ref. [16].

The reliability of the simulation results depends strongly on the accuracy of the used material model. A good model should account for at least the effects of strain, strain rate, and temperature. In the machining simulations, adiabatic heating of the material and the thermal softening with strain are also very important and should therefore be taken into account. One of the most commonly used material models is the one originally presented by Johnson and Cook (JC model) [17, 18]. The JC model presents the flow stress of the material as a function of strain, strain rate, and temperature. The function is shown in equation (1). Mathematically the flow stress is presented as a multiplication of three terms; the strain hardening, strain rate sensitivity, and temperature terms. The material constants in the JC model are determined by fitting the equation to measured data. The predictive power of this model without any modifications can be questioned. The extrapolation of strain, strain rate, and temperature can lead to unexpected results, as the mechanisms of plastic deformation can change when strain rate, for example, is increased. Furthermore, the ability of this model to simulate strain localization is limited. The simulations of adiabatic shear bands in high speed machining require the model to take into account the local thermal softening and simultaneous strain hardening of the material. In the JC model, thermal softening is governed by the exponent 'm' of equation (1), while strain hardening ($d\sigma/d\varepsilon$) is affected by several factors. With positive strain rate sensitivity (or parameter 'C'), the strain hardening rate increases with strain rate. Therefore, the localization becomes less likely when the strain rate and/or strain rate sensitivity are increased. For these reasons, there are numerous other models presented in the literature for various simulation purposes. Usually, however, the number of parameters increases rapidly as the accuracy of the model is increased. Lodykowski et al. [19] compared simulations of orthogonal cutting of ES mild

steel using the JC model (total of 14 physical and fitting parameters), the model presented by Rusinek and Klepaczko [20] (17 parameters), and the model presented by Perzyna [21] (28 parameters). According to their comparison, the results obtained with these three different models differ in details, but qualitatively the results were quite similar. However, reliable determination of the material model parameters becomes increasingly more difficult as the number of parameters increases. Therefore, despite its limitations, the JC model is still extremely useful due to its simplicity and availability of its parameters for many commercial metals and alloys.

$$\sigma = (A + B\varepsilon^n)\left(1 + C\ln\frac{\dot{\varepsilon}}{\dot{\varepsilon}_{ref}}\right)\left(1-\left[\frac{T-T_{ref}}{T_m-T_{ref}}\right]^m\right) \quad (1)$$

In this work, the numerical modeling of titanium and nickel based alloys was performed by characterizing the material behavior in compression. The experimental characterization was carried out in a wide range of strain rates and temperatures, and the Johnson–Cook model parameters were obtained from the measured data. For the Ti-6246 the simulations using the JC model gave reasonably good results, but for the nickel based superalloy the material model did not predict the plastic flow accurately. The equation for the superalloy was modified to better take into account the reducing strain hardening rate at large deformations and softening of the material during high speed machining. This modified model is shown to be able to simulate the adiabatic shear banding and the formation of the serrated chip in orthogonal cutting.

Experimental Procedure

The materials studied in this work were titanium-6246 alloy and a nickel-based superalloy 625. The chemical compositions of the alloys are presented in Tables 1 and 2. Ti-6246 is a high strength $\alpha + \beta$ alloy, whereas Alloy 625 is similar to the Inconel 625 superalloy. Both alloys were studied in a soft annealed condition, and no precipitates were present in the microstructure. Compression specimens of 6 mm in diameter and 6 mm to 8 mm in length were EDM machined from round bars with a diameter of 70 mm.

The material behavior was characterized in compression at temperatures ranging from room temperature up to 730 °C at strain rates ranging from 10^{-3} s^{-1} to 4600 s^{-1}. The low strain rate tests up to the strain rate of 1 s^{-1} were performed using an

Table 1 Chemical composition of the Ti-6246 alloy

	Ti	Al	Sn	Zr	Mo
Max wt%	Bal	6	2	4	6

Table 2 Chemical composition of the Alloy 625

	Ni	Cr	Fe	C	Mn	Si	Mo	Co	Al	Ti	Nb+Ta
Max wt%	Bal	23	5	0.03	0.5	0.4	10	1	0.4	0.4	3.8

MTS servohydraulic materials testing machine with an induction heating setup. The high strain rate tests, on the other hand, were performed using a Split Hopkinson Pressure Bar (SHPB) device with high temperature capabilities [22–24].

The Hopkinson Split Bar device used in this study comprises four maraging steel bars. i.e., striker, incident, transmitted, and momentum trap bars. All bars have the same diameter of 22 mm. The incident, transmitted, and momentum trap bars were 1,200 mm long each, while the length of the striker bar varied from 200 mm to 400 mm. The device itself, the dispersion correction method, and the calculations for obtaining the stress, strain, and strain rate in the sample are described in details in, for example, refs. [25–28].

The high strain rate tests at high temperatures were carried out using a special bar and specimen manipulation system enabling heating of the specimen while keeping the bars at room temperature. Keeping the bars at or close to room temperature is very important, because heating only a part of the bars would generate temperature gradients into the bars that could lead to locally different sound velocities. Also, the strength of the maraging bars could drop drastically if the bars were heated to too high temperatures. In the current high temperature system the specimen is inserted into a ceramic wool ring, which is further placed into a specimen holder arm. The specimen holder with the specimen inside the ceramic wool ring is then pneumatically moved into a small tube furnace located beside the bars. Once the specimen has reached the desired test temperature, the specimen holder arm quickly pulls the specimen back to the centerline of the bars. At this point, the hot specimen is not yet touching the cold bars and inside the ceramic wool ring its temperature decrease is still negligible. After the specimen has reached the centerline, the striker bar is shot and a second pneumatic actuator pushes the bars and the specimen into contact just a fraction of a second before the impact. With this system, the contact time of the hot specimen and the cold bars can be limited to less than 50 ms, which is short enough to limit the temperature loss in the specimen surface to just a few degrees [22–24]. Figure 1 shows the testing steps involved in a high temperature SHPB compression test.

Dynamic Behavior Tests

Compression Test Results for the Ti-6246 Alloy

Figure 2(a and b) show the compression stress–strain curves for Ti-6246 alloy at the strain rates of 1,600 s^{-1} and 2,800 s^{-1}

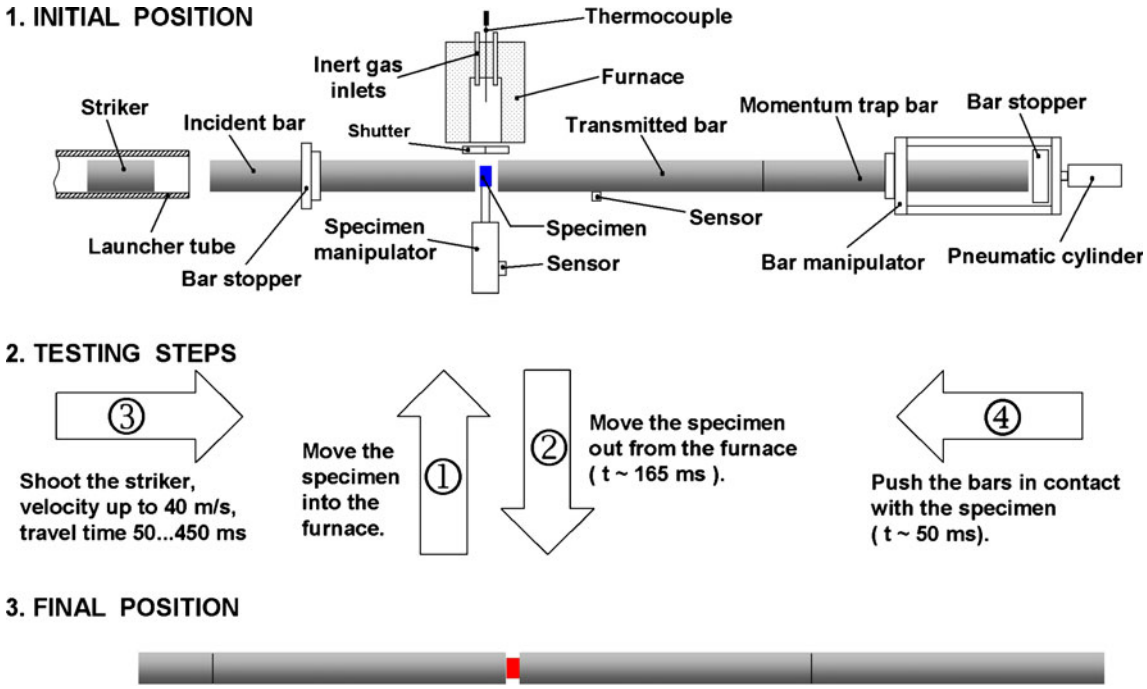

Fig. 1 Testing steps involved in the high temperature SHPB compression test

at temperatures ranging from room temperature to 600 °C. The material shows rather constant flow stresses as a function strain at both strain rates at all test temperatures. At room temperature the strength of the material at these two strain rates is basically the same, but at high temperatures some strain rate sensitivity can be observed as the strength of the material increases slightly with increasing strain rate. The flow stress of the material at 4 % of plastic strain is shown in Fig. 2(c) as a function of strain rate at different temperatures. The strain rate sensitivity in the low strain rate region is at room temperature rather high, but it quickly decreases when temperature is increased to 200 °C. With further increase in temperature, the strain rate sensitivity increases slightly but is still significantly lower than that observed at room temperature. The difference in the strength of the material between the high and low strain rate experiments is more prominent at elevated temperatures. The increase in the material's strength at room temperature over the strain rate region from 10^{-3} s^{-1} to 2,800 s^{-1} is approximately 16 %, while at 200 °C and 400 °C the strength increases by 33 % and 29 %, respectively. This behavior can be explained by stronger viscous drag effects on the dislocations at higher temperatures [29].

Compression Test Results for the Alloy 625

The results from the compression tests on Alloy 625 are shown in Fig. 3. At room temperature, Fig. 3(a), the yield strength of the material varies between 490 MPa at low strain rates and 690 MPa at the highest strain rate of 4,600 s^{-1}. At all strain rates, the flow stress increases almost linearly with strain and the strong strain hardening continues up to about 25 % of strain, after which it starts to slowly decrease. The strain hardening rate is also fairly insensitive to strain rate, which is not typical for most large grained FCC metals. For most FCC metals, the dominant significant strain rate sensitive deformation mechanism is cutting of forest dislocations, which increases with strain. This typically leads to higher strain rate sensitivity at larger deformations. For Alloy 625 this does not seem to be the case in the studied strain rate region, since the slope of the stress strain curve does not change with deformation. The strain hardening of FCC metals is a result of several processes, including reducing dislocation mobility due to increasing dislocation density and the following repulsive dislocation interactions, recovery of dislocations, and thermal softening due to adiabatic heating. For Alloy 625, the strain hardening is the same at all strain rates, and it therefore seems that the mechanisms increasing the strength and those decreasing the strength are somehow balanced at all strain rates in the studied strain rate region.

Figure 3(b) shows the stress–strain curves measured at the strain rate of 1,000 s^{-1} at different temperatures. No essential change in the overall response of the material is observed when the temperature is increased from room temperature to 200 °C apart from the yield behavior, which changes from smooth and continuous yielding to discontinuous and pronounced. This behavior could be explained by the

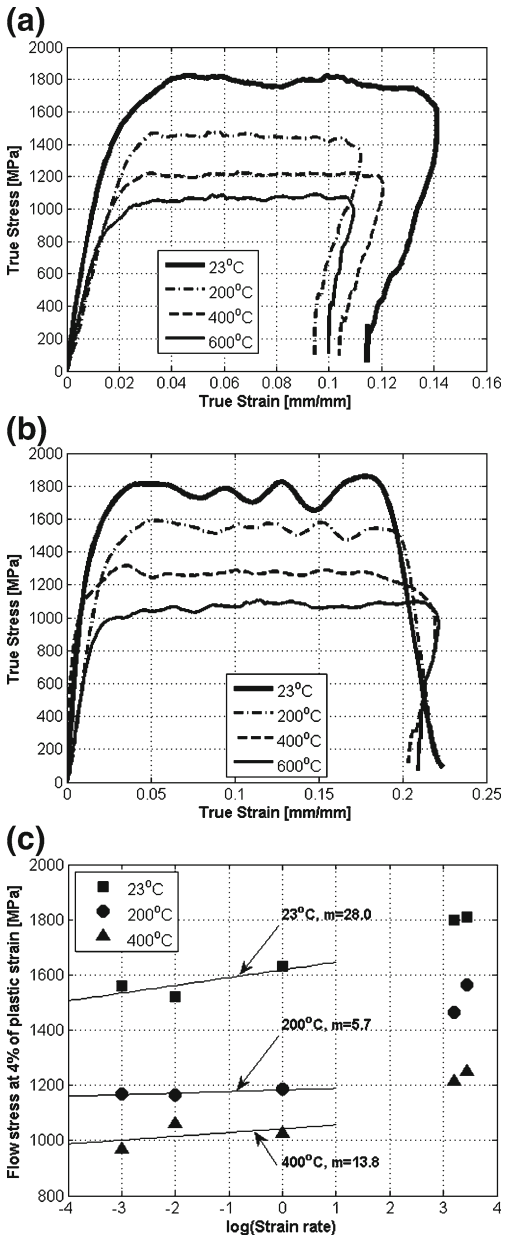

Fig. 2 Compression stress–strain curves for Ti-6246 alloy at (**a**) 1,600 s^{-1} and (**b**) 2,800 s^{-1}. (**c**) flow stress value at 4 % of plastic strain as a function of strain rate at different temperatures

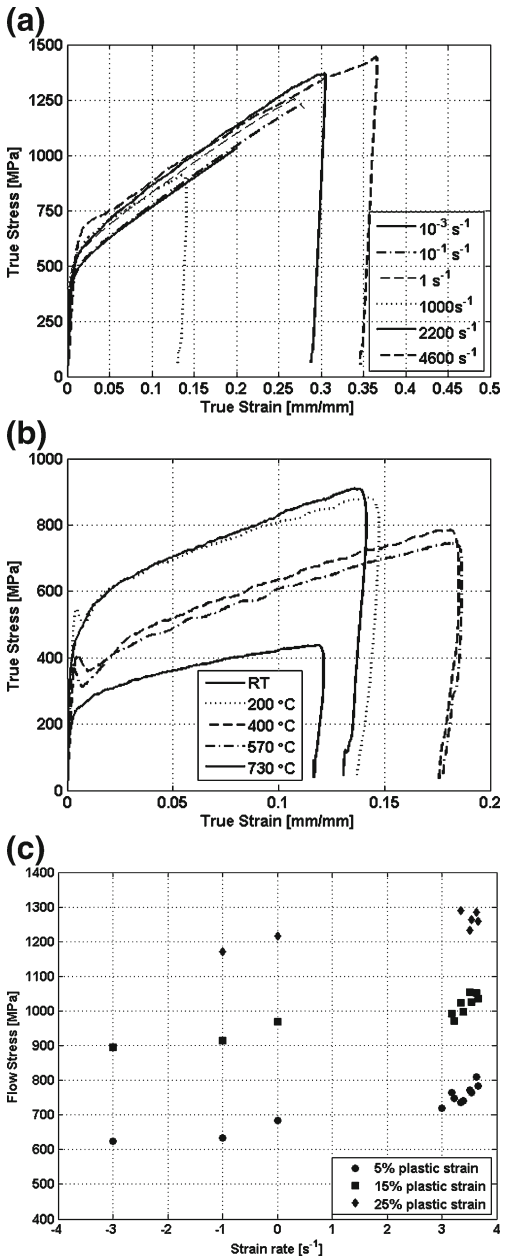

Fig. 3 Results from the compression tests on Alloy 625: (**a**) stress–strain curves measured at room temperature at different strain rates, (**b**) stress–strain curves measured at different temperatures at the strain rate of 1,000 s^{-1}, and (**c**) flow stress at 5, 15, and 25 % of plastic strain a function of logarithmic strain rate

increased diffusion of the alloy atoms into the dislocation cores and stacking faults, leading to higher initial yield strength followed by a breakage of dislocations from their pinning points and a decrease in the flow stress before smooth strain hardening sets in. It is also worth mentioning that the low strain rate tests at high temperatures showed clear serrated flow, which is an indication of dynamic strain aging during the test.

The strain rate sensitivity of Alloy 625 is presented in Fig. 3(c), where the room temperature flow stresses at different plastic strains are plotted as a function of strain rate. The strain rate sensitivity seems to be fairly constant with respect to strain. In the high strain rate region, above ~1,000 s^{-1}, the strain rate sensitivity seems to increase slightly with strain.

Modeling and Simulations

Modeling of the Mechanical Behavior of Ti-6246

The Johnson–Cook material model was used to for the modeling of mechanical behavior of the Ti-6246 alloy.

Table 3 Johnson-Cook model parameter values for the initial and optimized sets

Parameter	A [MPa]	B [MPa]	n	C	m	T_r [°C]	T_m [°C]	B	ρ [kg/m^3]	C_p [J/kgK]
Value (initial)	1866	901	0.7392	0.01	0.6962	23	1625	0.9	4650	508
Value (optimized)	1657	402	0.2180	0.0054	0.8034	23	1625	0.9	4650	508

The adiabatic stress was calculated using the model shown in equation (2).

$$\sigma_{adi} = (A + B\varepsilon^n)\left(1 + C\ln\frac{\dot{\varepsilon}}{\dot{\varepsilon}_{ref}}\right)\left(1-\left[\frac{T + \Delta T - T_{ref}}{T_m - T_{ref}}\right]^m\right) \tag{2}$$

Where ΔT is the adiabatic heating calculated using equation (3).

$$\Delta T = \frac{\beta}{\rho c}\int_0^{\varepsilon}\sigma d\varepsilon \tag{3}$$

The initial parameters for the model were acquired by first obtaining a reference stress–strain curve at 1,600 s^{-1} at room temperature. Then parameter m was calculated using equation (4), where the yield stresses ${\sigma_{T1}}^Y$ and ${\sigma_{T2}}^Y$ were determined from the stress–strain curves measured at 23 °C and 400 °C, respectively. The experimental (adiabatic) stress–strain curve obtained at the reference temperature was converted to the isothermal one using equation (5).

$$m = \log\left(1-\frac{\sigma_{T2}^Y}{\sigma_{T1}^Y}\right)\Big/\log\left(\frac{T_2 - T_{ref}}{T_m - T_{ref}}\right) \tag{4}$$

$$\sigma_{ISO} = \frac{\sigma_{ADI}}{1-\left(\frac{T+\Delta T-T_{ref}}{T_m - T_{ref}}\right)^m} \tag{5}$$

The parameters A, B, and n were obtained from the isothermal reference stress–strain curve by fitting the Ludvik equation, i.e., the first term in the Johnson-Cook model, to the data using a nonlinear least squares fit. Finally, the parameter C was obtained by visually comparing the calculated stress–strain curves with the experimental ones. The initial parameter set was then optimized using the Matlab function 'lsqcurvefit', which is a non-linear least square fitting routine, where the fitting can be done simultaneously to all measured stress–strain curves. This optimization was done using the

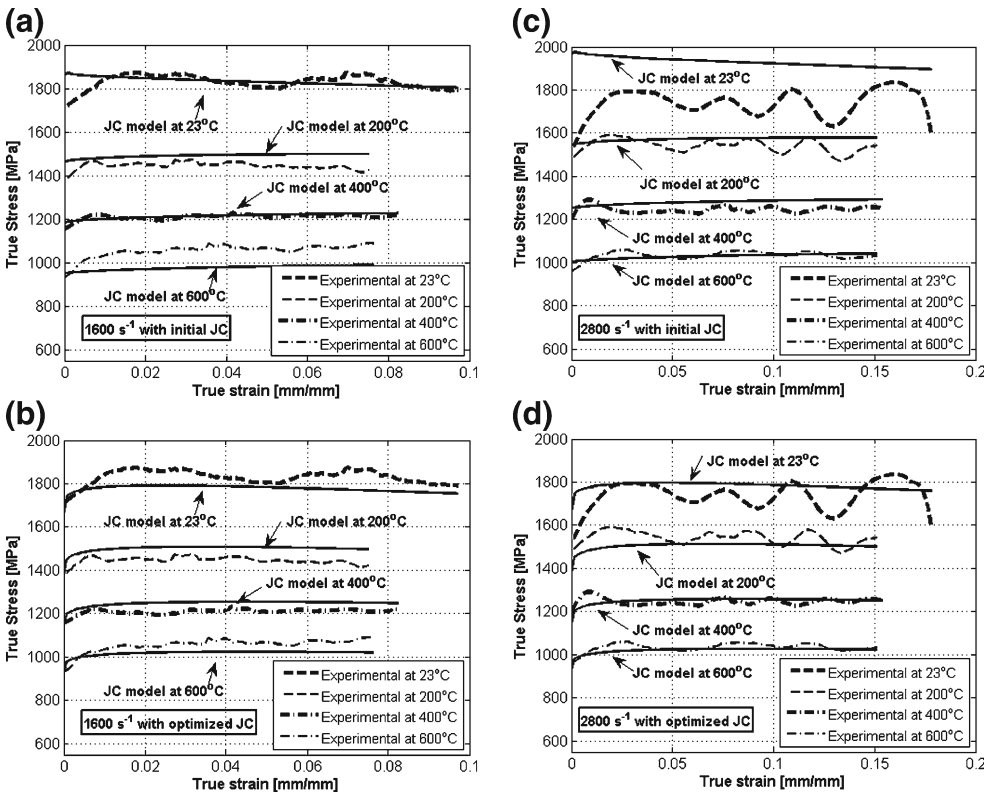

Fig. 4 Experimental data and data calculated using the JC model: (**a**) initial parameter set at 1,600 s^{-1}, (**b**) optimized parameter set at 1,600 s^{-1}, (**c**) initial parameter set at 2,800 s^{-1}, and (**d**) optimized parameter set at 2,800 s^{-1}

Table 4 The Johnson – Cook model parameter values for Alloy 625

Parameter	A [MPa]	B [MPa]	n	C	m	$\dot{\varepsilon}_{ref}$ [s^{-1}]	T_{ref} [°C]	T_m [°C]	C_p [J/kgK]	ρ [kgm^{-3}]
Value	558.8	2201.3	0.80	0.000209	1.146	1670	23	1350	480	8440

initial parameter set and the true stress vs. true plastic strain curves obtained from the compression test (Fig. 2(a and b)). Both the initial and optimized sets are shown in Table 3. The main differences in the two parameter sets are the clearly lower values of parameters B, n and C, and slightly higher value of the parameter m in the optimized parameter set.

The difference between the stress–strain curves calculated using initial and optimized parameter sets is shown in Fig. 4. The JC model with the initial parameter set (Fig. 4(a)) matches the experimental data at the reference conditions, i.e., at the strain rate of 1,600 s^{-1} at room temperature. The fit is also quite good at 400 °C, which was the temperature at which the thermal softening exponent 'm' was obtained. However, already at 600 °C the model clearly underestimates the experimental flow stresses. Also, the fit is poor at higher strain rates, where the model overestimates the room temperature strength. After optimization of the JC model parameters (Fig. 4(b)) the flow stresses at room temperature slightly decrease at 1,600 s^{-1} and increase at 400 °C and 600 °C, and the match between the experimental and calculated flow stresses is significantly improved at higher temperatures. Furthermore, the optimized JC model can predict the material response much better at higher strain rates (Fig. 4(d)) and is therefore more suitable for describing the material response in a wider range of strain rates and temperatures. The rapid decrease of adiabatic strength (equation (2)) with strain is also observed as the temperature of the material quickly rises with high rate deformation. Using this model, the simulated material temperature reaches 370 °C already at the strain of 50 %, and the melting temperature is reached at about 200 % of strain. Segmented chipping of the material was observed during preliminary cutting simulations without the use of additional damage models, which are required when strain hardening in the material model exceeds the thermal softening caused by adiabatic heating.

Modeling of the Mechanical Behavior of Alloy 625

The JC model parameter values for the Alloy 625 were found by using a nonlinear fitting routine in Matlab and assuming the deformation to be adiabatic. Similarly as for the titanium alloy, the fitting was done using the high strain rate stress–strain curves only as the lower strain rates are not likely to occur in high speed machining. The obtained parameter values are shown in Table 4, where relatively high values for parameters 'B' and 'n' indicate the strong strain hardening observed also in the experiments. On the other hand, the parameter 'C' has a very low value suggesting low strain rate sensitivity, which is not evident in the experiments, where positive strain rate sensitivity was observed (Fig. 3(c)). However, parameter 'C' in the JC model also describes the rate sensitivity of strain hardening, which for this material is very low. Therefore, the optimal fit between the JC model and the experimental data is obtained at essentially zero strain rate sensitivity. Comparison of the true material behavior with that predicted by the optimal JC model clearly shows one weakness

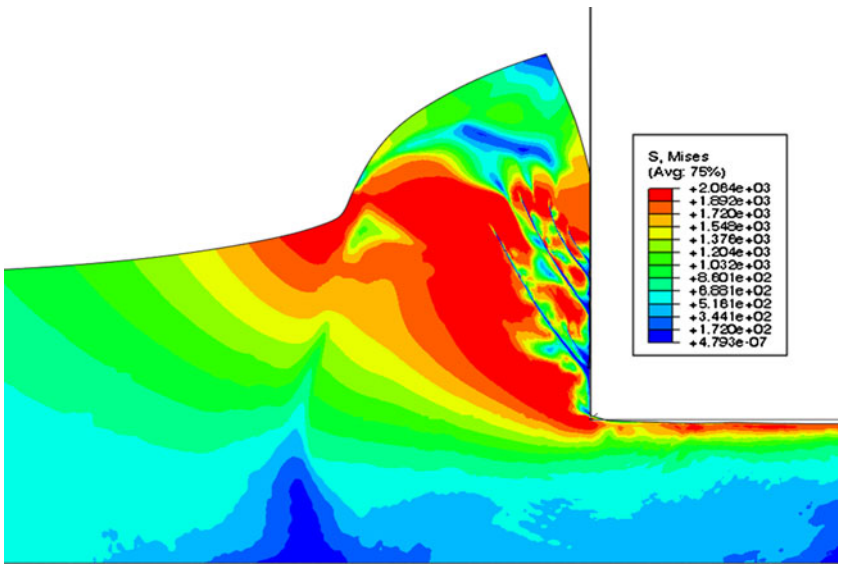

Fig. 5 Von Mises stress distribution in Alloy 625 chip formed using unmodified Johnson-Cook model (Table 4)

of the JC model: the strain rate sensitivity of the flow stress and the strain rate sensitivity of strain hardening, i.e., the slope of the stress strain curve, are affected by the same parameter. This model can be used to accurately describe the true material behavior of only such materials whose strain hardening increases with increasing strain rate. For Alloy 625 this is not the case as discussed in Chapter 3.2. For modeling the true material behavior of Alloy 625, the effect of strain rate on the flow stress should be separated from the effect that strain rate has on strain hardening. This way the simulated stress strain curve could retain its shape at different strain rates, and only the flow stress would increase with increasing strain rate.

The model is not able to account for the softening in the shear zones, mainly due to its very strong strain hardening term. Moreover, the simulated adiabatic stress–strain curve shows softening only at high strains so the simulations of orthogonal cutting using this model do not form segmented chips. In the simulations using this model (Fig. 5), the material deforms in front of the tool, and only some initial waviness is seen in the morphology of the chip, but the shear bands are arrested by the strong strain hardening imposed by the material model. Also, the cutting stresses obtained in the simulations were unreasonably high. With this model, the predicted strength of the material at high strains simply becomes too high. Therefore, the model was modified using an approach similar to that presented by Sima and Özel [13] and Calamaz et al.[14, 15], who used additional strain softening terms in the Johnson–Cook Equation. The Johnson–Cook model used for the simulations of Alloy 625 is shown in equation (6), where the parameter 'k' is the strain softening exponent that describes the strength of strain softening at large deformations.

$$\sigma_{adia} = (A + B\varepsilon^{n})\left(\tanh\left(\frac{1}{\varepsilon^{k}}\right)\right)\left(1 + C\ln\frac{\dot{\varepsilon}}{\dot{\varepsilon}_{ref}}\right)\left(1-\left[\frac{T + \left(\Delta T - T_{ref}\right.}{T_{m} - T_{ref}}\right]^{m}\right) \quad (6)$$

Figure 6(a) shows a comparison between the measured experimental data and the values calculated using the Johnson–Cook model (equation (5), with k=0). The fit at the strain rate of 3,500 s^{-1} at room temperature is very good. At higher temperatures, however, the model clearly overestimates the stress, but the fit is still reasonably good. Extrapolation of the stress—strain curve to higher strains and the effect of the strain softening parameter 'k' are shown in Fig. 6(b). Without the strain softening, the parabolic strain hardening function increases the flow stress to values over 2,000 MPa at strains above 0,8. The simulation results using this unmodified model (equation (6), with k=0) for cutting simulations are shown in Fig. 5. The strain hardening rate in the model can, however, be reduced using the strain softening exponent. Strain softening exponent k=1 decreases the maximum stress from about 2,150 MPa to about 1,650 MPa. Increasing the strain softening exponent to k=2.0 and k=3.0 actually increases the peak stress, but the softening at strains higher than the maximum stress is significantly stronger than that observed for smaller values of k. For k=3.00, the strength of the material decreases to about 350 MPa at the strain of 2. Furthermore, the added strain softening term has only one extra parameter, it does not essentially affect the simulated flow stresses at small strains, and the match between the experimental data and the simulated values is essentially the same with or without the strain softening term.

Machining Simulations

ABAQUS 6.9-1 software was used to create the two dimensional explicit finite element model and for the simulations of

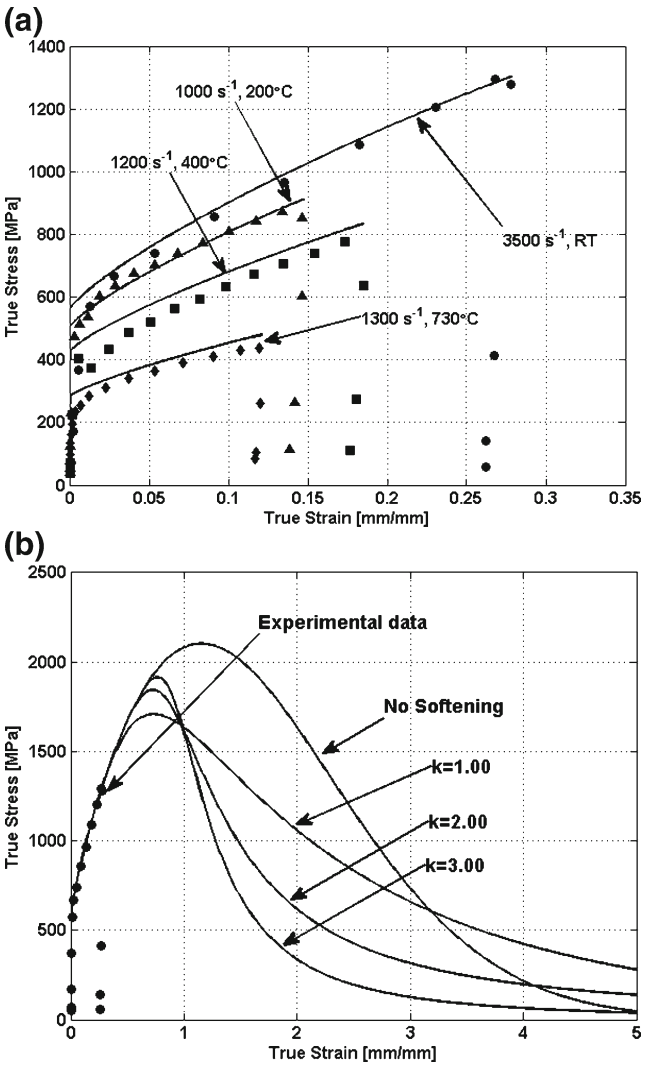

Fig. 6 (**a**) experimental data and the values predicted by the unmodified Johnson–Cook model (equation (6), with k=0), (**b**) the stress–strain curves extrapolated up to 500 % of strain using different values of k

orthogonal cutting. In the simulations, the heat conduction from the chip to the tool was not allowed and a conservative friction coefficient of 0.1 was used between the tool and the chip. The finite element model is shown in Fig. 7, where very fine meshing was used for the workpiece. In total, the model contained 101151 nodes and 100049 elements. A sacrificial layer was used to model the separation of the chip from the workpiece. For the titanium alloy the elements in the separation layer were simply deleted after the elements reached the shear strain of 2.0. For the Alloy 625, however, the isotropic hardening model was implemented in the simulation model using the VUHARD Fortran routine. Material states such as equivalent plastic strain, equivalent plastic strain rate, and the temperature were provided by the solver. Stress values were given by the material model as long as the material point was deforming. A linear damage evolution model was used to model the element deletion. The element damage starts at a damage initiation strain (ε_0^d=1.5) and after reaching the critical failure strain (ε_{fail}=2.0) the element is deleted. The linear damage evolution model with the damage variable 'd' is given in equation (7).

$$d = \frac{\varepsilon - \varepsilon_0^d}{\varepsilon_{fail} - \varepsilon_0^d} \tag{7}$$

As a result, the adiabatic stress during damage becomes:

$$\sigma_{adia} = (1-d)\sigma_{adia} \tag{8}$$

In the current material model for Alloy 625, however, the essentially zero strain rate sensitivity and the added strain softening lead to excess softening of the sacrificial layer leading to rapid crack growth along the layer. For these reasons, the strain rate sensitivity of the material model was assumed to increase at extreme strain rates and the parameter 'C' of the Johnson-Cook model was calculated using equation (9).

$$C(\dot{\varepsilon}) = C\left(1 + 200*\left(1-\exp\left(^{-(\dot{\in}-\dot{\varepsilon}_0)}/_{\dot{\varepsilon}_C}\right)\right)\right) \tag{9}$$

In equation (9), C is the strain rate sensitivity parameter of the unmodified model $\dot{\in}$ the strain rate, $\dot{\in}_0$ is the reference strain rate of the model, and $\dot{\in}_C$ is a constant with a value of $10^5\ s^{-1}$. Equation (9) was not used at strain rates lower than the reference strain rate, where the constant value of C presented in Table 2 was used to describe the strain rate sensitivity. In the simulations, equation (9) was used to model the material behavior in both the separation layer and in the chip. The increasing strain rate sensitivity prevents the catastrophic crack propagation in the separation layer, but it also prevents strain localizations in the chip. Therefore, equation (9) was used for all strains in the separation layer, but in the chip it was only used for strains higher than 1.5 mm/mm. Ideally the material behavior should be simulated in the chip and in the separation layer using the same model. This problem needs further attention and will be taken into account in the future work on finite element modeling of this material.

It should be emphasized that the changes made to the material models and the overall modeling approach presented in this paper have no clear physical background and should be considered only as a mathematical way to improve the simulation accuracy.

Cutting Experiments

The simulation results were compared with the results obtained from cutting experiments done with the Hopkinson

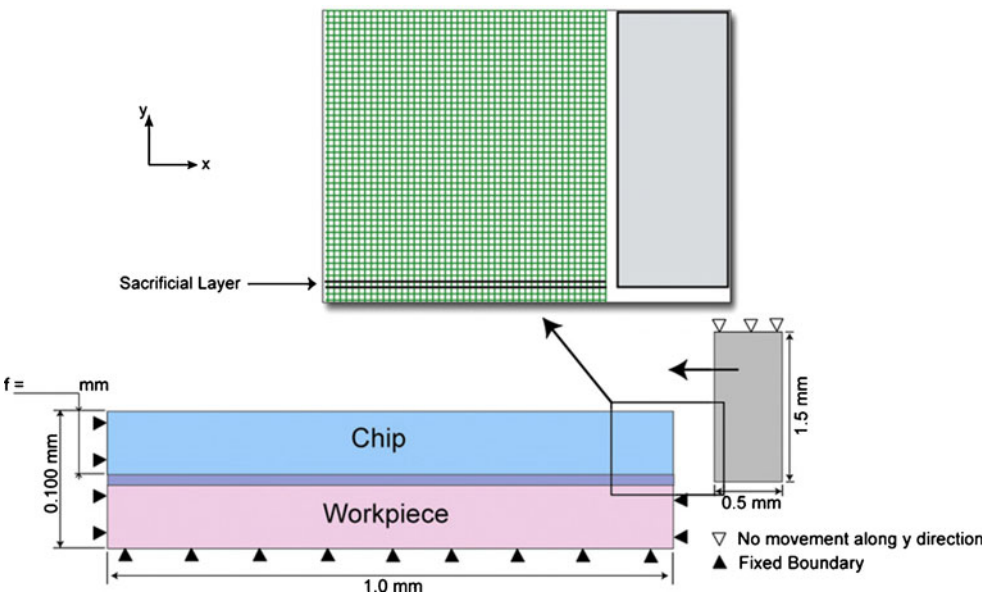

Fig. 7 The finite element model used in the orthogonal cutting simulations of Ti-6246 and Alloy 625

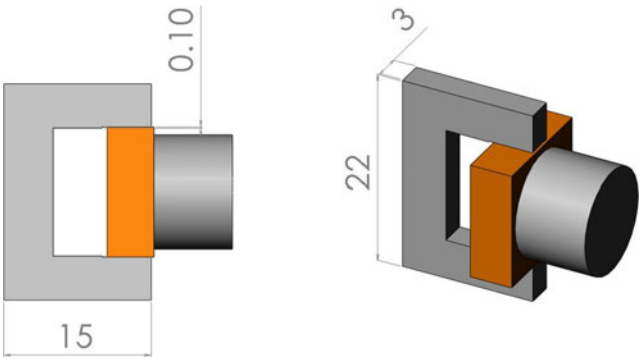

Fig. 8 Schematic picture of the U-shape specimen and the tool. Units are in millimeters

Split Bar device using U-shape specimens. In these experiments, a square tool is inserted between the arms of a U-shape specimen, and the tool-specimen assembly is simply placed between the incident and transmitted bars of the Hopkinson Split Bar device so that the tool holder rests against the incident bar and the bottom of the 'U' against the transmitted bar. A schematic picture of the U-shape tool—specimen assembly is shown in Fig. 8. The experiment is performed by impacting the striker bar to the free end of the incident bar and by measuring the cutting forces from the transmitted bar. The cutting depth was measured from optical micrographs obtained after the experiment. In this experiment, however, the tool impacts the specimen several times due to the back-and-forth traveling residual stress wave in the incident bar. Also, the contact of the tool with the bottom of the 'U' can severely distort the chip shape and also damage the tool and the tool holder (Fig. 9(d)). Therefore, the chip that is recovered after the experiment is not perfectly comparable with the

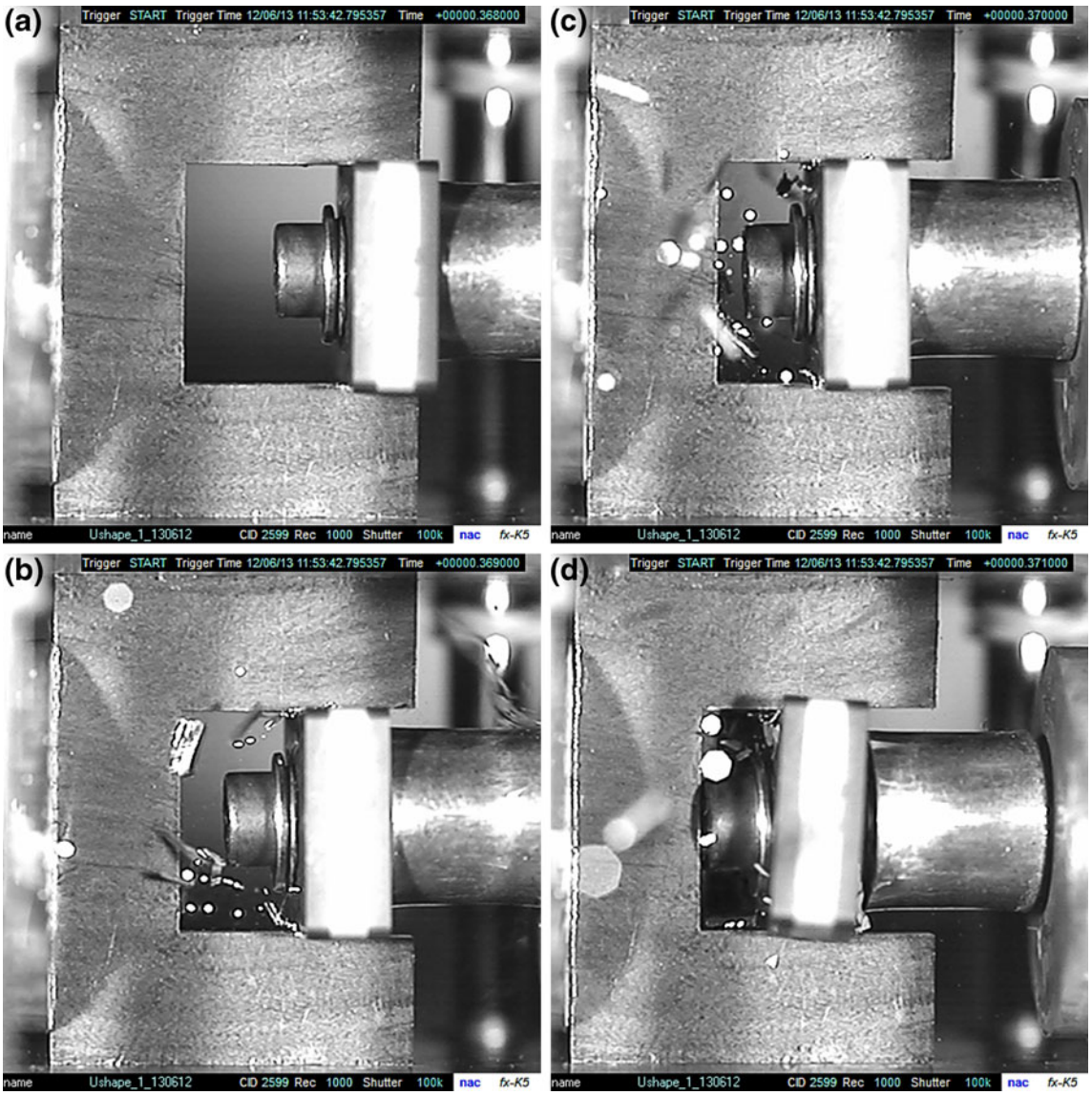

Fig. 9 High-speed camera images of a Hopkinson Split Bar cutting experiment with the U-shape sample (**a**–**d**)

simulated one. The comparison between the simulated and experimentally obtained chips presented in this paper are based on the chips recovered from the U-shape cutting experiments (Fig. 9), but also on the chips recovered from quick-stop experiments performed at Technische Universität Braunschweig. An example of a chip recovered from the U-shape test on titanium 6246 is shown in Fig. 10. Unfortunately, the chips that would match exactly with the simulated cutting conditions were not available, and because of this, a very conservative approach was chosen for the discussion concerning the comparison of the chips.

The preliminary results from the simulations of orthogonal cutting are shown in Fig. 11. The material models are clearly able to produce segmented chips that are also observed in high speed machining of these alloys. A more detailed inspection of the shear bands in the material show splitting of the shear bands near the tool edge, which is also observed experimentally. Overall shape of the chip, however, as well as the fine details, such as the thickness of individual serrations, are somewhat different from those observed in the experiments. The simulations and experiments were performed at the same cutting conditions. For Ti-6246 the cutting depth was 0.2 mm and cutting speed 15 m/s, whereas for Alloy 625 the cutting depth was 47 μm and cutting speed 13 m/s. The experimentally obtained cutting stresses for Ti-6246 and Alloy 625 were 1500 MPa and 1620 MPa, respectively. The corresponding cutting stresses obtained from the simulations were 1750 MPa for Ti-6426 and 1930 MPa for Alloy 625. The overestimated cutting forces in the simulations are most likely due to the overestimated strength of the materials at large deformations. Overall, even though the chips produced by the simulations are clearly segmented, the material model used in the simulations needs to be further developed in order to improve the consistency between simulated and measured cutting forces and the details of the chip shape such as the thickness of individual segments.

Conclusions

The mechanical behavior of titanium-6246 and a nickel based superalloy were thoroughly investigated at a wide range of strain rates and temperatures. The experimental data was used to obtain Johnson-Cook material model parameters, and the models were used for simulating orthogonal cutting. The simulation results were compared to the results obtained from cutting experiments.

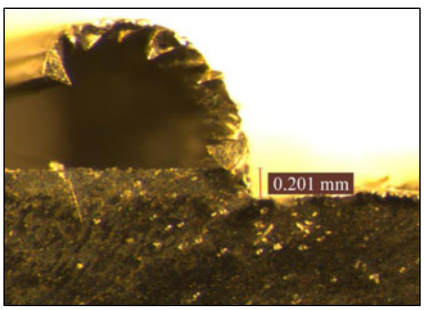

Fig. 10 Example of a chip recovered from the U-shape cutting experiment at the cutting speed of 15 m/s for Ti-6246

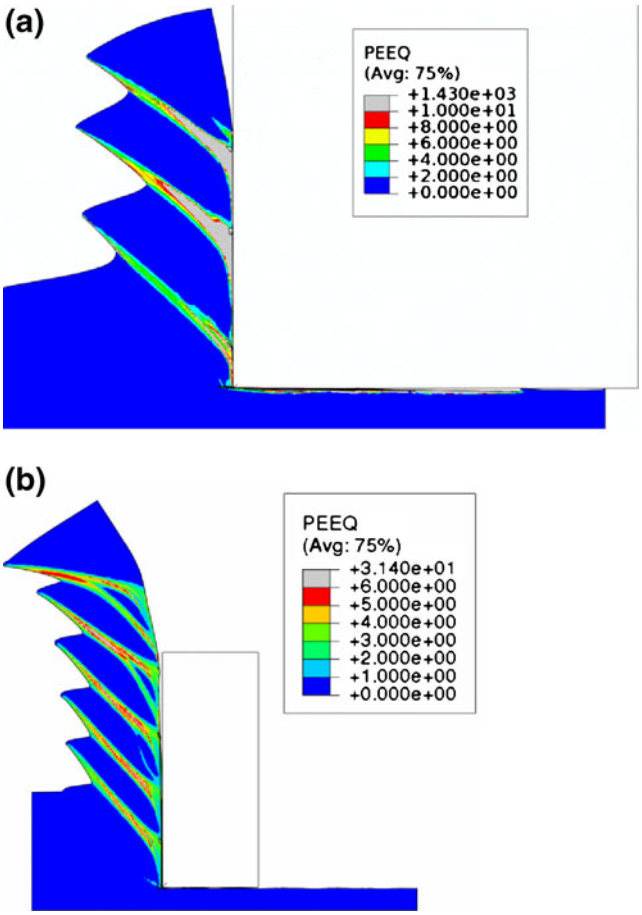

Fig. 11 The simulated chip shape and plastic equivalent strain for (**a**) Alloy 625 and (**b**) Titanium-6246

The mechanical behavior of the Ti-6246 alloy is characterized by high strength and relatively low strain hardening. The strain hardening decreases with increasing strain rate due to the strong adiabatic heating. For Alloy 625, on the other hand, the strain hardening is very strong and essentially independent of strain rate.

For both materials, only high strain rate data was used for obtaining the parameters, since the low strain rates are not likely to occur during machining. The parameters used in the simulations for the titanium alloy were obtained by first manually fitting the model to the experimental data, and then optimizing the fit using non-linear fitting algorithms in Matlab. For the Alloy 625, the parameters were obtained simply using a similar non-linear fitting routine in Matlab. However, this material model did not produce acceptable simulation results, since the model overestimates the strength of the material at high strains due to the strong parabolic

hardening of the material model. Furthermore, the best fit to the experimental data was obtained at essentially zero strain rate sensitivity. The zero strain rate sensitivity of the model can reproduce the shape of the stress strain curve at different strain rates, but it fails to model the increase of the flow stress with increasing strain rate. For these reasons, the material model for Alloy 625 was modified for better simulation accuracy. A strain softening term was added to the Johnson-Cook material model that allows the simulated strength of the material to be decreased at large deformations. The strain rate sensitivity of the material model was also modified so that at very high strain rates the sensitivity could be increased.

For both materials, the simulated cutting stresses were higher than the experimental values. The differences between the simulated and experimental cutting stresses were most likely due to the overestimated strength of the material at large deformations, and the different friction conditions in the simulations and experiments. Both material models were able to simulate chip segmentation and shear banding, and the material model for Alloy 625 even produced spit shear bands that were also observed in the experimental chips. However, the overall shape of the chip and its fine details were not a perfect match with the experimentally obtained chips, and more work is needed to further improve the simulation accuracy. One promising method for improving the modeling and simulation accuracy is the inverse parameter determination from the cutting experiments [30].

Acknowledgments The research leading to these results has received funding from the European Union Seventh Framework Programme (FP7/2007-2013) under grant agreement No. PITN-GA-2008-211536, project MaMiNa.

References

1. Ezugwu EO, Bonney J, Yamane Y (2003) An overview of the machinability of aeroengine alloys. J Mater Process Technol 134:223–252
2. Ezugwu EO, Wang ZM, Machado AR (1999) The machinability of nickel-based alloys: a review. J Mater Process Technol 86:1–16
3. Fang N, Wu Q (2009) A comparative study on the cutting forces in high speed machining of Ti-6Al-4V and Inconel 718 with a round cutting edge tool. J Mater Process Technol 209:4385–4389
4. Costes JP (2007) Tool-life an wear mechanisms of CBN tools in machining of Inconel 718. Int J Mach Tool Manuf 47:1081–1087
5. Dudzinski D, Devillez A, Moufki A, Larrouquere D, Zerrouki V, Vigneau J (2004) A review of developments towards dry and high speed machining of Inconel 718. Int J Mach Tool Manuf 44:439–456
6. Wang ZY, Rajurkar KP, Fan J, Lei S, Shin YC, Petrescu G (2003) Hybrid machining of Inconel 718. Int J Mach Tool Manuf 43:1391–1396
7. Mitrofanov AV, Ahmed N, Babitsky VI, Silberschmidt VV (2005) Effect of lubrication and cutting parameters on ultrasonically assisted turning of inconel 718. J Mater Process Technol 162–163:649–654
8. Ahmed N, Mitrofanov AV, Babitsky VI, Silberschmidt VV (2006) Analysis of material response to ultrasonic loading in turning Inconel 718. Mater Sci Eng A 424:318–325
9. Dong G, Zhaopeng H, Rongdi H, Yanli C, Muguthu J (2011) Study of cutting deformation in machining nickel-based alloy Inconel 718. Int J Mach Tool Manufacture 51:520–527
10. Ulhmann E, Graf von der Schulenburg M, Zettier R (2007) Finite element modeling and cutting simulations of Inconel 718. Ann CIRP 56:1
11. Ortiz M, Quigley JJ (1991) Comput Methods Appl Mech Eng 90:781–804
12. Marusich T, Ortiz M (1995) Int J Numer Methods Eng 38:3675–3694
13. Sima M, Özel T (2010) Int J Mach Tool Manuf 50:943–960
14. Calamaz M, Coupard D, Girot F (2008) Int J Mach Tool Manuf 48:275–288
15. Calamaz M, Coupard D, Girot F (2010) Mater Sci Technol 14:244–257
16. Vaz M, Owen DR, Kalhori V, Lundblad M, Lindgren L (2007) Arch Comput Methods Eng 14(2):173–204
17. Johnson G, Cook W (1983) In the Proceedings of the 7th International Symposium on Ballistics
18. Johnson G, Cook W (1985) Int. J. Eng Fract Mech
19. Lodygowski T, Rusinek A, Jankowiak T, Sumelka W (2012) Eng Trans 60:69–96
20. Rusinek A, Klepaczko J (2001) Int J Plast 17:87–115
21. Perzyna P (2008) Mechanics 27:25–42
22. Apostol M (2007) Ph.D. thesis, Tampere University of Technology
23. Apostol M, Kuokkala V-T, Vuoristo T (2004) In: Papalettere C (ed) Advances in Experimental Mechanics. McGraw-Hill, Bari Italy
24. Apostol M, Vuoristo T, Kuokkala V-T (2003) J de Phys IV 110
25. Gorham D (1983) J Phys E: Scientific Instruments, 16.
26. Hokka M, Kuokkala V-T, Curtze S, Vuoristo T, Apostol M (2006) J de Phys 134
27. Hokka M, Leemet T, Shrot A, Baeker M, Kuokkala V-T (2012) Mater Sci Eng A 550:350–357
28. Vuoristo T (2004) Ph.D. thesis, Tampere University of Technology
29. Meyers M (1994) Dynamic Material Behavior. John Wiley and Sons, USA
30. Shrot A, Bäker M (2012) Determination of Johnson-Cook parameters from machining simulations. Comput Mater Sci 52:298–304